

# Exciton-assisted optomechanics with suspended carbon nanotubes

I Wilson-Rae<sup>1,2\*</sup>, C. Galland<sup>3</sup>, W. Zwerger<sup>2</sup>, A. Imamoglu<sup>3</sup>

<sup>1</sup>Institute for Theoretical Physics, Universität Erlangen-Nürnberg, D-91058 Erlangen, Germany

<sup>2</sup>Technische Universität München, D-85748 Garching, Germany

<sup>3</sup>Institute of Quantum Electronics, ETH Zürich, Wolfgang-Pauli-Strasse 16, CH-8093 Zürich, Switzerland

E-mail: \*Ignacio.Wilson-Rae@ph.tum.de

**Abstract.** We propose a framework for inducing strong optomechanical effects in a suspended carbon nanotube based on deformation potential exciton-phonon coupling. The excitons are confined using an inhomogeneous axial electric field which generates optically active quantum dots with a level spacing in the milli-electronvolt range and a characteristic size in the 10 nm range. A transverse field induces a tunable parametric coupling between the quantum dot and the flexural modes of the nanotube mediated by electron-phonon interactions. We derive the corresponding excitonic deformation potentials and show that this interaction enables efficient optical ground-state cooling of the fundamental mode and could allow us to realise the strong and ultra-strong coupling regimes of the Jaynes-Cummings and Rabi models.

## 1. Introduction

The realisation of the quantum regime of a macroscopic mechanical degree of freedom [1, 2] has emerged as a natural goal from considering the fundamental limits for the measurement of small forces and displacements [3, 4, 5, 6, 7]. This achievement could provide a versatile alternative for the exploration of the quantum-to-classical transition and the development of quantum technologies. Recent progress in the implementation of optomechanical [4, 5, 6, 7] and electromechanical [3] microsystems and nanosystems, has already enabled access to this regime [8, 9, 10, 11, 12]. Some critical requirements in this respect are: (i) quantum limited measurement of the transduced output, (ii) sufficiently low effective masses, and (iii) sufficiently low mechanical dissipation. Optomechanical schemes are ideally suited to meet (i) given the availability of shot-noise limited photodetection. In turn suspended single-walled carbon nanotubes (CNTs) [13] are emerging as unique candidates to meet criteria (ii) and (iii) [14, 15]. Indeed recent transport experiments in these systems have demonstrated strong coupling of charge to vibrational resonances [16, 17, 18] and mechanical quality-factors ( $Q$ ) exceeding  $10^5$  for resonant frequencies approaching 1 GHz [19]. Thus, implementing optomechanical systems based on suspended CNTs would represent a significant milestone.

The standard paradigm in optomechanics is based on an optical cavity whose frequency is modulated by the motion of one of its mirrors or of a dielectric object inside it via radiation pressure effects [4, 5, 6]. Though recently this approach has been successfully carried over to nanoresonators with subwavelength dimensions [20, 21, 22], it becomes inefficient for high-frequency resonators ( $\gtrsim 1$  GHz) with low polarisabilities like sub-micron CNTs. Here we propose a promising alternative based on a way of inducing coherent optomechanical transduction that exploits the unique properties of excitons in CNTs [23, 24, 25, 26]. The role of the optical cavity is played by an excitonic resonance of the CNT that couples parametrically to the flexural motion via deformation potential electron-phonon interactions [27, 28]. Homodyne detection of the in-phase component of the output field of the resonantly driven two-level emitter afforded by the excitonic resonance allows then to perform a continuous measurement of the mechanical displacement. This procedure, which could be implemented using the differential transmission technique [29], is akin to ion-trap measurements [30] and analogous to cavity-assisted schemes [31]. However a two-level emitter is a highly nonlinear system, in stark contrast to an optical cavity mode, and this feature provides an additional motivation for our proposal given the potential it offers for the demonstration of non-classical motional states of the CNT. In fact, a major advantage of this particular mechanical resonator-exciton system with respect to prior scenarios [32] is the possibility of realising a mechanical analogue of the strong-coupling regime of cavity-QED [33, 34] with a vacuum Rabi splitting in the 100 MHz range.

As shown in Fig. 1, we envisage a suspended neutral semiconducting CNT where the centre of mass (CM) of the exciton is localised via the spatial modulation of the Stark-shift induced by a static inhomogeneous electric field. We analyse a tip-

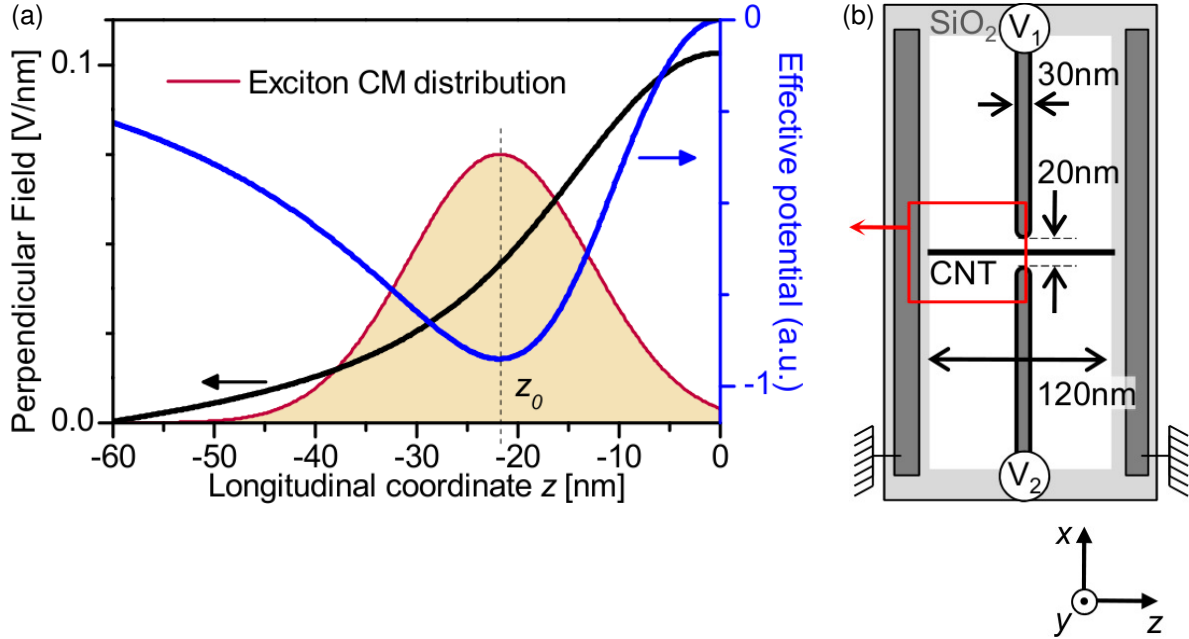


**Figure 1.** (a) Perpendicular field  $E_{\perp}(z)$ , effective confining potential  $V_{\text{eff}}^{(00)}(z)$ , and resulting exciton CM probability distribution (a.u.) in the harmonic approximation for  $V_1 = -0.75$  V and  $V_2 = 1.75$  V—the tailored confinement generates a double well with minima at  $|z| = z_0$  [ $E_{\parallel}(z_0) = 9.6\text{V}\mu^{-1}$  and inter-well tunnelling is negligible]. (b) Schematic view of the device (both the tip electrodes and the CNT are suspended). Here we consider the restrictions imposed on the fields by the need to avoid sizable static deflections (cf. Sec. 3.2), field emission (the maximum field at the tip electrodes is approximately  $200\text{V}\mu^{-1}$ ) and dielectric breakdown, and assume for simplicity cylindrical symmetry around the tips’ axis.

electrode configuration that effectively engineers a pair of tunable optically active nanotube quantum dots (NTQDs) with excitonic level spacing in the meV range implying a confinement length below 10 nm. The quantum confinement is induced by the inhomogeneity in the field component along the CNT axis  $E_{\parallel}$ . In turn the normal component  $E_{\perp}$  breaks the axial symmetry inducing a tunable parametric coupling between the exciton and the in-plane flexural motion of the CNT. This allows for optical ground-state cooling [35, 36, 32, 11] of the fundamental mode at an ambient temperature in the Kelvin range.

Another aspect of the CNT systems proposed here is their relevance in the broader context of quantum photonics applications. The optical manipulation of single carriers trapped at well-defined and repeatedly addressable locations has proved invaluable to probe the foundations of quantum mechanics and constitutes a key resource for enabling quantum technologies. In this respect solid state zero-dimensional optical emitters offer a promising alternative to realisations based on trapped atoms. Examples of such systems are semiconductor quantum dots [37], rare-earth doped crystals [38, 39], NV colour centres in diamond [40, 41] and, more recently, the system considered here, i.e. excitons in semiconducting CNTs [24]. For the latter photon antibunching

has already been observed and there is indirect evidence that exciton localisation arises spontaneously [24], probably as a result of charged defects in the surrounding matrix or disorder in the CNT. Naturally, in view of the aforementioned quantum applications it would be desirable to artificially tailor exciton confinement in a controlled fashion in an ultra-clean suspended CNT. However the band-gap engineering approach deployed for this purpose in more standard semiconductor materials is hardly viable for CNTs. Suspension is motivated by the need to (i) avoid substrate-induced fluorescence quenching and (ii) control the enhanced phonon-induced optical dephasing that results from the one-dimensional nature of this system.

We will first present in Sec. 2 a suitable model for the CNT excitons that will be used to analyse both their quantum confinement generating the NTQD and their interaction with CNT low-frequency phonons, as modified by the applied electrostatic fields. Subsequently, in Sec. 3, we will consider the axial phonon confinement induced by the finite CNT suspended length and derive an effective model for the fundamental in-plane flexural-phonon mode coupled to the NTQD. Finally, also in Sec. 3, this effective model will be used to describe optomechanical effects induced when the NTQD is driven by a laser — e.g. the possibility of efficient laser cooling of the fundamental mode close to its motional quantum ground state.

## 2. Exciton effective model

The electronic structure of a CNT can be understood in terms of graphene rolled into a seamless cylinder. In graphene, the conduction and valence bands cross at two inequivalent “Dirac points” in the reciprocal lattice [42] ( $K$  and  $K'$ ). The corresponding effective ( $k \cdot p$ ) Dirac Hamiltonian reads

$$H_D = \hbar v_F (k_{x'} \hat{\sigma}_{x'} + k_{y'} \hat{\tau}_3 \hat{\sigma}_{y'}) , \quad (1)$$

where  $\hat{\sigma}_i$  [ $\hat{\tau}_i$ ] are Pauli matrices in sublattice ( $A$ - $B$ ) space [valley ( $K$ - $K'$ ) space] and  $v_F \approx 10^6 \text{ ms}^{-1}$  is the Fermi velocity. Here we follow the representation used by Ando [43] in which the Dirac spinor is expressed in terms of Bloch amplitudes as  $(\psi_A^K, \psi_B^K, \psi_A^{K'}, -\psi_B^{K'})$ . A rotation by the CNT’s chiral angle  $\theta$  is performed to align  $\hat{y}'$  with the nanotube axis ( $\hat{y}' \rightarrow \hat{z}$ ) —henceforth, we adopt cylindrical coordinates. Thus, the unit vectors in sublattice and valley space correspond to graphene 2D Bloch functions with wavevector  $K$  [ $K'$ ]:  $(1, 0, 0, 0)$  [ $(0, 0, 1, 0)$ ] is constructed from  $p_z$  orbitals centred at the  $A$  sites with phase  $e^{-i\theta/2}$  [ $e^{i\theta/2}$ ] at the central site, while  $(0, 1, 0, 0)$  [ $(0, 0, 0, 1)$ ] has the  $p_z$  orbitals centred at the  $B$  sites with phase  $e^{i\theta/2}$  [ $-e^{-i\theta/2}$ ] at the central site [42]. After folding, the resulting periodic boundary conditions imply that a wide-gap semiconducting nanotube is obtained when the nanotube indices satisfy  $\text{mod}(2n' + m', 3) \neq 0$ . The associated subband electronic 1D Bloch functions for  $k_z = 0$

are given by

$$|K_{n,\pm}\rangle \doteq \frac{e^{i(n-\nu/3)\varphi}}{\sqrt{4\pi}} \begin{pmatrix} \text{sgn}[3n - \nu] \\ \pm 1 \\ 0 \\ 0 \end{pmatrix}, \quad |K'_{n,\pm}\rangle \doteq \frac{e^{i(n+\nu/3)\varphi}}{\sqrt{4\pi}} \begin{pmatrix} 0 \\ 0 \\ \text{sgn}[3n + \nu] \\ \pm 1 \end{pmatrix}, \quad (2)$$

with single-particle eigenenergies

$$\epsilon_{n,\pm} = \pm \frac{\hbar v_F}{R} \left| n - \frac{\nu}{3} \right|, \quad \epsilon'_{n,\pm} = \pm \frac{\hbar v_F}{R} \left| n + \frac{\nu}{3} \right|. \quad (3)$$

Here  $+$  and  $-$  label, respectively, the conduction and valence bands, the index  $n$  corresponds to the quantisation of the single-particle azimuthal momenta ( $n = 0, \pm 1, \pm 2, \dots$ ),  $\nu = 2 \bmod(2n' + m', 3) - 3 = \pm 1$  denotes the type of semiconducting CNT [44],  $R$  is the CNT radius, and  $\varphi$  is the azimuthal angular coordinate (cf. Fig. 1).

The  $K - K'$  degeneracy, implied by Eqs. (2) and (3), and the electron spin yield for the lowest-energy exciton manifold a sixteen-fold degeneracy in the lowest order  $k \cdot p$  approximation provided by Eq. (1). This degeneracy is partially split by inter-valley mixing and exchange effects [43]. In the absence of a magnetic field there is a single bright level $\ddagger$ : the singlet bonding direct exciton  $|KK^*\rangle + |K'K'^*\rangle$  which typically has the highest energy [45] (here the conjugated wavefunctions correspond to the hole). Threading through the cross section a small Aharonov-Bohm flux  $\phi_{AB}$  renders the antibonding state  $|KK^*\rangle - |K'K'^*\rangle$  weakly allowed [43] so that its spontaneous emission rate can be tuned by varying the magnetic field. Note that the zero field splitting between the states  $|KK^*\rangle \pm |K'K'^*\rangle$  has been observed to be in the 1 meV range [26].

Henceforth, we will mainly focus on the  $E_{11}$  excitons  $|KK^*\rangle \pm |K'K'^*\rangle$  and consider their deformation potential (DP) coupling to the low-frequency acoustic phonons of the CNT in the presence of weak static electric fields. There are four phonon branches whose frequency vanishes with the wavevector, namely: compressional (stretching), torsional and two flexural (bending) branches. However relevant exciton-phonon interactions will only affect the compressional branch and the flexural branch polarised along  $\hat{x}$ . Indeed, the excitonic wavefunctions of interest are non-degenerate and, in the absence of a magnetic field (i.e. for  $\phi_{AB} = 0$ ), the field configuration in Fig. (1) has reflection symmetry with respect to the  $xz$  plane. Thus, the torsional branch and the flexural branch polarised along  $\hat{y}$ , which are antisymmetric with respect to this reflection operation, are decoupled.

To obtain a tractable model for the excitonic wavefunction suitable for analysing the CM confinement of the exciton and its coupling to acoustic phonons, we adopt a phenomenological approach based on: (i) the aforementioned  $k \cdot p$  graphene zone-folded scheme following Ando [43, 46] but neglecting inter-subband transitions (cf. Refs. [47, 48]), and (ii) an envelope function approximation within each subband with the parametrisation developed in Refs. [44, 48] (based on a comparison of tight binding and *ab initio* approaches) but the Bloch function at  $K, K'$  as determined by

$\ddagger$  Note however that manipulating the indirect excitons may also be viable [25].

(i) and assuming electron-hole symmetry. In line with this last assumption we take for the effective mass associated to a given subband the average of the electron and hole effective masses obtained in Ref. [44]. This framework neglects the impact of curvature effects on the Bloch functions but allows to incorporate realistic values for the effective masses of electrons and holes [44] and for the exciton Bohr radius [48] —here the Bloch functions mainly play a role in determining the selection rules. In the absence of external fields, this leads to the following singlet direct exciton wavefunctions

$$|\psi_{nm\pm}\rangle = \frac{1}{2} (|K_{n,+}K_{m,-}^*\rangle \otimes |F_{nm}\rangle \pm |K'_{-m,+}K'^*_{-n,-}\rangle \otimes |F'_{nm}\rangle) \otimes (|\uparrow\downarrow\rangle + |\downarrow\uparrow\rangle), \quad (4)$$

where the envelope functions  $|F_{nm}\rangle, |F'_{nm}\rangle$  satisfy  $F_{nm}(z_e, z_h) = F'_{nm}(z_h, z_e)$ . Here we use that the single-particle eigenenergies  $\epsilon_{n,+}$  ( $\epsilon_{n,-}$ ) and  $\epsilon'_{-n,+}$  ( $\epsilon'_{-n,-}$ ) are degenerate and inter-valley mixing preserves the total orbital momentum and angular momentum along  $\hat{z}$ . One should note that in general Eq. (4) implies entanglement between the valley and orbital degrees of freedom but for axially-symmetric excitons such that  $n = m$ , the envelope functions differ at most by a  $\pi$ -phase so that they factor out and the axial degrees of freedom become disentangled ( $n = m = 0$  for  $E_{11}$  excitons).

### 2.1. Exciton confinement

We turn now to the analysis of the quantum confinement of the exciton's CM motion induced by an applied inhomogeneous electrostatic field. The symmetric tip electrode configuration sketched in Fig. 1 with voltages  $V_1$  and  $V_2$  allows independent tuning of  $E_\perp$  and  $E_\parallel$  as the reflection symmetries imply that their magnitudes are determined, respectively, by  $(V_2 - V_1)/2$  and  $(V_2 + V_1)/2$ . In order to generate a Stark-shift induced excitonic quantum dot, we consider parameters such that the length scale over which  $E_\perp$  and  $E_\parallel$  vary appreciably is much larger than the CNT radius  $R$  (i.e. they can be regarded as constant across the CNT's cross section) and larger than the excitonic Bohr radius. It follows that for sufficiently weak magnitudes (see below): (i) the effect of  $E_\parallel$  is dominated by intrasubband virtual transitions whose effect on the CM motion can be treated adiabatically, while (ii)  $E_\perp$  leads to a perturbation  $\propto e^{\pm i\varphi}$  that only induces intersubband virtual transitions.

More precisely, the effect of the external fields on the exciton can be described by the following interaction Hamiltonian

$$\hat{V} = \hat{V}_\parallel + \hat{V}_\perp \quad (5)$$

with

$$\hat{V}_\parallel = e [U(0, \hat{z}_h) - U(0, \hat{z}_e)] \quad (6)$$

and

$$\hat{V}_\perp = \frac{e}{\epsilon_\perp} [\hat{x}_e E_\perp(\hat{z}_e) - \hat{x}_h E_\perp(\hat{z}_h)]. \quad (7)$$

Here  $U(x, z)$  is the external electrostatic potential (in the plane  $y = 0$ ), so that  $E_{\parallel}(z) = -\frac{\partial U}{\partial z}(0, z)$  and  $E_{\perp}(z) = -\frac{\partial U}{\partial x}(0, z)$ , and  $\epsilon_{\perp} \approx 1.6$  denotes the intrinsic relative permittivity normal to this axis [49]. Given that the depolarisation effect only affects the perpendicular field and the fact that the typical level spacing between the relevant excitonic states arising from a given pair of subbands  $n, m$ , is smaller than the intersubband energy spacing, we can assume that the Stark-shift induced CM confinement will be dominated by  $\hat{V}_{\parallel}$  and neglect  $\hat{V}_{\perp}$  in this subsection §. Then, for each pair of subbands  $n, m$ , we perform the substitution

$$z_{e/h} = z_{\text{CM}} \mp \frac{\mu}{m^{(n/m)}} z' \quad (8)$$

with inverse

$$z_{\text{CM}} = \frac{m^{(n)}z_e + m^{(m)}z_h}{m^{(n)} + m^{(m)}}, \quad z' = z_h - z_e, \quad (9)$$

where  $m^{(n)}$  ( $m^{(m)}$ ) is the effective mass of subband  $n$  ( $m$ ) and  $\mu = m^{(n)}m^{(m)}/(m^{(n)} + m^{(m)})$  is the excitonic reduced mass. Here the indices  $n, m$  refer to the  $K$  point and the corresponding envelope function is enough to determine the wavefunction [cf. Eq. (4)] —note that an analogous substitution can be performed for the  $K'$  point and  $m^{(-n)} = m^{(n)}$ . The aforementioned smoothness of the fields implies  $\langle \hat{z}_{\text{CM}}^2 \rangle \gg \langle \hat{z}'^2 \rangle$  so that substituting Eq. (8) into Eq. (6) and Taylor expanding we obtain a linear potential

$$\hat{V}_{\parallel} = e\hat{z}' \frac{\partial U}{\partial z}(0, \hat{z}_{\text{CM}}) + \mathcal{O}[\hat{z}'^2]. \quad (10)$$

We now consider  $E_{\parallel}(z)$  much smaller than the critical field to ionise the exciton so that the relevant intrasubband matrix elements of  $\hat{V}_{\parallel}$  are much smaller than the binding energy. The latter warrants for the ground state manifold of the excitonic hydrogenic series [50] associated to  $n, m$ , a description in terms of an effective Hamiltonian by adiabatic elimination of the corresponding excited manifolds. Naturally, the corresponding states have well-defined parity. Thus, this effective Hamiltonian for the CM motion has a potential part whose leading contribution is second order in  $\hat{V}_{\parallel}$ . From Eq. (10) we obtain for this effective confining potential

$$V_{\text{eff}}^{(nm)}(z_{\text{CM}}) = -\alpha_X^{(nm)} E_{\parallel}^2(z_{\text{CM}}), \quad (11)$$

where

$$\alpha_X^{(nm)} = e^2 \sum_{l \neq 0} \frac{|\langle f_{eh,0}^{(nm)} | \hat{z}' | f_{eh,l}^{(nm)} \rangle|^2}{E_l^{(nm)} - E_0^{(nm)}} \quad (12)$$

is the corresponding excitonic polarisability. Here we have introduced the wavefunctions  $\{|f_{eh,l}^{(nm)}\rangle\}$  on the relative coordinate  $z'$  for the hydrogenic series  $l = 0, 1, \dots$  arising from  $n, m$ . In a classical picture, the field polarises the exciton that thus experiences a force

§ More precisely, for  $E_{\parallel}(z_0) \sim E_{\perp}(0)$  the relative order of the transverse field's contribution to the effective confining potential would be given by  $\xi \mathcal{E}_* \frac{R}{\sigma_{eh}} \sim 10^{-3}$  for relevant nanotube parameters (cf. Eq. (18) and Secs. 2.2 and 3.1).

proportional to the gradient of the squared field. If one considers the characteristic level spacings

$$E_l^{(nm)} - E_0^{(nm)} \sim \frac{e^2}{8\pi\epsilon_0\epsilon_{n-m}(0)\sigma_{eh}^{(nm)}} \quad (13)$$

and the order of the relevant matrix elements  $\sim \sigma_{eh}^{(nm)}$  (where  $\sigma_{eh}^{(nm)}$  is the exciton Bohr radius and  $\epsilon_{n-m}(q)$  an appropriate dielectric function [43]), it follows from Eq. (12) that the excitonic polarisability is of order

$$\alpha_X^{(nm)} \sim 8\pi\epsilon_0\epsilon_{n-m}(0)\sigma_{eh}^{(nm)3}. \quad (14)$$

Here  $\epsilon_0(0) = \epsilon_{\parallel} \approx 7$  corresponds to the intrinsic relative permittivity along the CNT axis [49].

We focus now on  $E_{11}$  excitons so that  $n = m = 0$ . To determine the electrostatic potential generated by the aforementioned symmetric tip electrode configuration, we have performed FEM calculations with COMSOL multiphysics for relevant parameters (cf. Sec. 3.1). We assume for simplicity cylindrical symmetry around the tips' axis so that the ground electrode corresponds to a cylindrical shell with diameter approximately equal to the CNT length  $L$  (cf. Fig. 1). To model this configuration with electrodes of length  $L_T \gg L$  we consider Neumann boundary conditions at  $|x| = L_*$  with  $L_*$  smaller but comparable to  $L_T$  (i.e.  $E_x = 0$  for  $|x| = L_* \sim 1 \mu$ ). The effective confining potential  $V_{\text{eff}}$  is then estimated from Eqs. (11) and (14). As expected it vanishes at the origin and is given by a double well with minima at  $|z| = z_0$ , comparable to the distance between the tip electrodes (i.e. the tailored confinement generates a QD molecule). For typical parameters, it is permissible to neglect inter-well tunnelling and use in our estimates the harmonic approximation for the ground state of each well. We consider as a representative example a (9, 4) CNT,  $E_{\parallel}(z_0) = 9.6 \text{ V}\mu^{-1}$  and  $z_0 = 21 \text{ nm}$  (cf. Fig. 1). This results in an excitonic CM zero point motion  $\sigma_{\text{CM}}^{(00)} \sim 9 \text{ nm}$  (corresponding to  $\sigma_{\text{eh}}^{(00)} \approx 1.5 \text{ nm}$  [48] and  $m_{\text{CM}} = 0.2m_e$  [44], with  $m_e$  the electron mass in vacuum) and a level spacing  $\Delta E \sim 2 \text{ meV}$  —where  $\frac{\partial^2 E_{\parallel}}{\partial z^2}(z_0)$  is taken from the FEM calculation. Alternatively, heuristic considerations imply that the curvature at the well minima is of order  $|V_{\text{eff}}^{(nm)}(z_0)|/z_0^2$  which, together with Eqs. (11) and (14), yields

$$\sigma_{\text{CM}} \sim \frac{\sqrt{\hbar z_0/E_{\parallel}(z_0)}}{2 [2\pi m_{\text{CM}}\epsilon_0\epsilon_{\parallel}\sigma_{\text{eh}}^3]^{1/4}} \quad (15)$$

and

$$\Delta E \sim \frac{\hbar E_{\parallel}(z_0)}{2z_0} \sqrt{\frac{2\pi\epsilon_0\epsilon_{\parallel}\sigma_{\text{eh}}^3}{m_{\text{CM}}}} \quad (16)$$

where we have omitted the subband superscripts. Given the subwavelength separation between the wells, for each doublet only the symmetric state is bright so that the degeneracy is irrelevant. Thus, the wavefunctions for relevant  $E_{\parallel}$  are well approximated by the form given in Eq. (4) with a suitable envelope function

$$F_{nm}(z_e, z_h) = f_{eh}^{(nm)}(z_h - z_e) f_{\text{CM}}\left(\frac{m^{(n)}z_e + m^{(m)}z_h}{m^{(n)} + m^{(m)}}\right) \quad (17)$$

[cf. Eq. (9)], and for the ground state of the  $E_{11}$  bonding (antibonding) manifold, henceforth denoted by  $|\psi_{00+}\rangle$  ( $|\psi_{00-}\rangle$ ), we take both functions  $f_{\text{CM}}$  and  $f_{eh}$  to be Gaussian [48].

Finally, more precise criteria to warrant the above adiabatic treatment are given by

$$(i) \quad |E_{\parallel}(z_0)| \ll e/8\pi\epsilon_0\epsilon_{\parallel}\sigma_{eh}^2 \equiv \mathcal{E}_* \quad \text{and} \quad (ii) \quad z_0 \gg \sigma_{eh}; \quad (18)$$

which follow, respectively, from requiring that the relevant matrix elements of  $\hat{V}_{\parallel}$  be much smaller than the corresponding unperturbed energy differences [cf. Eq. (13)] and that the variation of the fields be smooth enough  $\parallel$ . This second condition (ii) is necessary, together with (i), to ensure

$$\Delta E \ll E_l^{(nm)} - E_0^{(nm)} \quad \text{or alternatively} \quad \sigma_{\text{CM}} \gg \sigma_{eh}, \quad (19)$$

which justifies the Taylor expansion leading to Eq. (10), and can be obtained using Eqs. (11), (13), (14), (15) and (16) together with the assumptions  $\sigma_{eh} \sim 4\pi\epsilon_0\epsilon_{\parallel}\hbar^2/\mu e^2$  and  $\mu \sim m_{\text{CM}}$ .

## 2.2. Field-induced exciton-phonon coupling

In what follows we will first consider the influence of the transverse field  $E_{\perp}$  on the ground state of the  $E_{11}$  axially-polarised exciton, which will amount to a slight hybridisation with the cross-polarised excitonic states, and then proceed to derive the corresponding excitonic deformation potentials in the presence of the applied fields.

To this end we treat the effect of  $\hat{V}_{\perp}$  on  $|\psi_{00\pm}\rangle$  to lowest order in perturbation theory. In principle the linear correction  $|\psi_{00\pm}^{(1)}\rangle$  involves contributions from all four excitonic manifolds for which  $|n| = 1$ ,  $m = 0$  or  $n = 0$ ,  $|m| = 1$ , namely  $E_{12}$ ,  $E_{21}$ ,  $E_{13}$  and  $E_{31}$ . It is straightforward to determine the necessary single-particle matrix elements of  $\hat{x}$  within our model for the excitonic wavefunctions, provided that the 2D “lattice contributions” (on the folded graphene sheet) are first reduced to momentum matrix elements which can be read out from the  $k \cdot p$  Hamiltonian (1). To this effect one can first consider the CNT as a 1D lattice so that there is only a “lattice contribution” to the matrix elements. Given that the operators  $\hat{x}$  and  $\hat{p}_x$  are well-behaved on the corresponding Bloch functions (which have finite range in the transverse directions) we can apply the standard relation between their matrix elements

$$\langle K_{m,\pm} | \hat{x} | K_{n,\pm} \rangle = \frac{i\hbar \langle K_{m,\pm} | \hat{p}_x | K_{n,\pm} \rangle}{m_e (\epsilon_{n,\pm} - \epsilon_{m,\pm})} \quad (20)$$

reducing the problem to the evaluation of matrix elements of  $\hat{p}_x$  ¶ — analogous relations hold for states at  $K'$ . We now use: (i)  $\hat{p}_x = \cos\hat{\varphi}\hat{p}_r - \sin\hat{\varphi}\hat{p}_{\varphi}$ , (ii) that  $\Pi$ -orbitals have

¶ We note that  $\mathcal{E}_*$  is comparable to the axial critical field for exciton dissociation and yields  $\sim 50 \text{ V}\mu^{-1}$  for relevant CNT parameters (cf. Sec. 3.1).

¶ Note that the validity of Eq. (20) hinges on the fact that homogeneous boundary conditions are satisfied for  $x, y \rightarrow \pm\infty$ , and this relation between matrix elements breaks down for periodic boundary conditions as those satisfied along  $z$ .

reflection symmetry with respect to the graphene sheet so that they do not carry  $\hat{p}_r$ , and (iii) that for Bloch functions near the Dirac points  $\hat{p}_\varphi \rightarrow m_e v_F \hat{\sigma}_{x'} - \frac{i\hbar}{R} \frac{\hat{\partial}}{\partial \varphi}$ . These, together with Eqs. (3) and (20) imply

$$\langle K_{m,\pm} | \hat{x} | K_{n,\pm} \rangle = \frac{\mp i \langle K_{m,\pm} | \sin \hat{\varphi} \left( R \hat{\sigma}_{x'} - \frac{i\hbar}{m_e v_F} \frac{\hat{\partial}}{\partial \varphi} \right) | K_{n,\pm} \rangle}{|n - \nu/3| - |m - \nu/3|}. \quad (21)$$

Subsequently, from Eqs. (2), (3) and (21), and using that  $\nu = \pm 1$  implies

$$\begin{aligned} \text{sgn}[3n - \nu]|_{n=\mp\nu} &= \mp\nu, & \text{sgn}[3n - \nu]|_{n=0} &= -\nu, \\ \frac{i}{2\pi} \int_0^{2\pi} d\varphi e^{i\nu\varphi} \sin \varphi &= -\frac{\nu}{2}, & \int_0^{2\pi} \frac{d\varphi}{2\pi} e^{i\frac{4\nu}{3}\varphi} \sin \varphi \frac{\partial}{\partial \varphi} e^{-i\frac{\nu}{3}\varphi} &= \frac{1}{6}, \end{aligned} \quad (22)$$

and that

$$\hat{\sigma}_{x'} |K_{0,\pm}\rangle = \mp\nu |K_{0,\pm}\rangle, \quad \hat{\sigma}_{x'} |K_{-\nu,\pm}\rangle = \mp\nu |K_{-\nu,\pm}\rangle; \quad (23)$$

we obtain

$$\langle K_{-\nu,\pm} | \hat{x} | K_{0,\pm} \rangle = \frac{R}{2} \pm \frac{\hbar}{6m_e v_F}, \quad \langle K_{+\nu,\pm} | \hat{x} | K_{0,\pm} \rangle = 0. \quad (24)$$

In turn, Eqs. (2) and (3) imply that the substitution  $\nu \rightarrow -\nu$  yields for the states  $|K'_{n,\pm}\rangle$  and  $|K'_{m,\pm}\rangle$ , expressions analogous to Eqs. (21), (22), (23) and (24) so that

$$\langle K'_{+\nu,\pm} | \hat{x} | K'_{0,\pm} \rangle = \frac{R}{2} \pm \frac{\hbar}{6m_e v_F}, \quad \langle K'_{-\nu,\pm} | \hat{x} | K'_{0,\pm} \rangle = 0. \quad (25)$$

Finally, from Eqs. (4), (7), (24), and (25), and using that  $\hat{x}$  is invariant under time reversal; it is straightforward to obtain

$$\begin{aligned} \langle \psi_{-\nu 0 \mp}^{(0)} | \hat{V}_\perp | \psi_{00\pm}^{(0)} \rangle &= -\langle \psi_{0-\nu\mp}^{(0)} | \hat{V}_\perp | \psi_{00\pm}^{(0)} \rangle = \frac{eR}{2\epsilon_\perp} \langle F_{-\nu 0} | E_\perp(\hat{z}_e) | F_{00} \rangle, \\ \langle \psi_{-\nu 0 \pm}^{(0)} | \hat{V}_\perp | \psi_{00\pm}^{(0)} \rangle &= \langle \psi_{0-\nu\pm}^{(0)} | \hat{V}_\perp | \psi_{00\pm}^{(0)} \rangle = \frac{\hbar e}{6\epsilon_\perp m_e v_F} \langle F_{-\nu 0} | E_\perp(\hat{z}_e) | F_{00} \rangle, \\ \langle \psi_{\nu 0 \mp}^{(0)} | \hat{V}_\perp | \psi_{00\pm}^{(0)} \rangle &= \langle \psi_{0\nu\mp}^{(0)} | \hat{V}_\perp | \psi_{00\pm}^{(0)} \rangle = \langle \psi_{\nu 0 \pm}^{(0)} | \hat{V}_\perp | \psi_{00\pm}^{(0)} \rangle = \langle \psi_{0\nu\pm}^{(0)} | \hat{V}_\perp | \psi_{00\pm}^{(0)} \rangle = 0, \end{aligned} \quad (26)$$

where we have used

$$F_{nm}(z_e, z_h) = F'_{nm}(z_h, z_e), \quad (27)$$

and that for a suitable choice of phases [cf. Eq. (17)]

$$F_{nm}(z_e, z_h) = F_{mn}(z_h, z_e). \quad (28)$$

Thus the contribution from  $|\psi_{\nu 0 \pm}^{(0)}\rangle$  ( $|\psi_{0\nu\pm}^{(0)}\rangle$ ) corresponding to  $E_{12}$  ( $E_{21}$ ) vanishes identically and, to first order in perturbation theory, we obtain for the admixture of cross-polarised excitons to the states  $|\psi_{00\pm}\rangle$  induced by  $E_\perp$

$$|\psi_{00\pm}^{(1)}\rangle \approx -\xi \sum_l \left( |\psi_{-\nu 0 \mp, l}^{(0)}\rangle - |\psi_{0-\nu\mp, l}^{(0)}\rangle + \zeta |\psi_{-\nu 0 \pm, l}^{(0)}\rangle + \zeta |\psi_{0-\nu\pm, l}^{(0)}\rangle \right) \langle F_{-\nu 0, l} | E_\perp(\hat{z}_e) | F_{00} \rangle, \quad (29)$$

where  $\xi \equiv eR/2\epsilon_\perp(E_{13} - E_{11})$ ,  $\zeta \equiv \hbar/3m_e v_F R$  and  $l$  labels a complete set of envelope functions for the  $E_{13}$  and  $E_{31}$  manifolds. Here we have assumed for the latter that

those having appreciable overlap with  $|F_{00}\rangle$  correspond to excitons with energies well approximated by the lowest one ( $E_{13} = E_{31}$ ) and have neglected the splitting between the bonding and antibonding manifolds. Note that these manifolds are likely to consist of delocalised electron-hole pair like states as is the case with the  $E_{33}$  band so that the analysis in section 2.1 may not apply [51]. However our treatment of  $E_{\perp}$  relies only on the validity of Eqs. (4) and (28) irrespective of the specific form of the envelope functions  $F_{-l0,l}$ , and on satisfying the weakness criterion  $|\xi E_{\perp}(z_0)|^2 \ll 1$ .

The Hamiltonian describing the interaction between electrons and low-frequency phonons has two distinct terms: (i) a deformation potential contribution diagonal in sublattice space corresponding to an energy shift of the Dirac point,

$$\hat{H}_{e\text{-ph}}^{(1)} = g_1 [\hat{u}_{\varphi\varphi}(\hat{r}) + \hat{u}_{zz}(\hat{r})] , \quad (30)$$

and (ii) a bond-length change contribution off-diagonal in sublattice space [27, 28] that in the Dirac picture emulates a gauge field,

$$\begin{aligned} \hat{H}_{e\text{-ph}}^{(2)} = g_2 \{ & (\cos 3\theta \hat{\sigma}_{x'} \hat{\tau}_3 - \sin 3\theta \hat{\sigma}_{y'}) [\hat{u}_{\varphi\varphi}(\hat{r}) - \hat{u}_{zz}(\hat{r})] \\ & - (\sin 3\theta \hat{\sigma}_{x'} \hat{\tau}_3 + \cos 3\theta \hat{\sigma}_{y'}) 2\hat{u}_{\varphi z}(\hat{r}) \} . \end{aligned} \quad (31)$$

Here  $g_1 \approx 30$  eV is the deformation potential constant,  $g_2 \approx 1.5$  eV the off-diagonal electron-phonon coupling constant [27, 28], and  $\hat{x}, \hat{y}$  only act on the ‘‘orbital’’ part of the 1D Bloch functions (cf. Eq. 2). The single-particle Hamiltonians (30) and (31) naturally lead to the following excitonic two-particle Hamiltonian <sup>+</sup>

$$\hat{H}_{X\text{-ph}} = \hat{\mathbb{P}}_e \hat{H}_{e\text{-ph}} \hat{\mathbb{P}}_e \otimes \hat{\mathbb{I}}_h - \hat{\mathbb{I}}_e \otimes \hat{\mathbb{P}}_h \hat{H}_{e\text{-ph}} \hat{\mathbb{P}}_h \quad (32)$$

where  $\hat{H}_{e\text{-ph}} = \hat{H}_{e\text{-ph}}^{(1)} + \hat{H}_{e\text{-ph}}^{(2)}$  and  $\hat{\mathbb{P}}_e$  ( $\hat{\mathbb{P}}_h$ ) denotes the projector on the conduction (valence) band.

Given that the relevant phonon modes have wavelengths,  $2\pi/q$ , that are much larger than the CNT radius,  $R$ , one can describe them using a continuum shell model [27, 52], with  $\hat{u}_{ij}(\hat{r})$  the corresponding Lagrangian strain operator, and keeping only the lowest orders in  $qR$  [27, 52] which amounts to the use of thin rod elasticity (TRE) [53]. Within this approximation, both compressional and flexural deformations have the structure of a local stretching so that the strain components satisfy  $u_{\varphi z} = 0$ ,  $u_{\varphi\varphi} = -\sigma u_{zz}$  with the latter given, respectively, by

$$u_{zz} = -R \cos\varphi \frac{\partial^2 \phi_f}{\partial z^2} \quad \text{and} \quad u_{zz} = \frac{\partial \phi_c}{\partial z} , \quad (33)$$

where  $\phi_f(z)$  [ $\phi_c(z)$ ] is the flexural [compressional] 1D field [53] that satisfies the Euler-Bernoulli [classical-wave] equation and  $\sigma = 0.2$  is a Poisson ratio for the CNT [52]. Finally, we consider the lowest order contributions in the external field (zeroth order in  $\phi_{AB}$ ) to the interaction between the lowest bright exciton states  $|\psi_{00\pm}\rangle \approx |\psi_{00\pm}^{(0)}\rangle + |\psi_{00\pm}^{(1)}\rangle$  of the NTQD and low-frequency phonons, i.e.

$$\langle \psi_{00\pm} | \hat{H}_{X\text{-ph}} | \psi_{00\pm} \rangle \approx \langle \psi_{00\pm}^{(0)} | \hat{H}_{X\text{-ph}} | \psi_{00\pm}^{(0)} \rangle + 2\Re \left[ \langle \psi_{00\pm}^{(0)} | \hat{H}_{X\text{-ph}} | \psi_{00\pm}^{(1)} \rangle \right] . \quad (34)$$

<sup>+</sup> As in Eq. (29), here we assume that only contributions involving virtual transitions to single exciton states are relevant.

Naturally, the axial angular momentum is preserved by coupling to compressional phonons and modified by interactions with flexural phonons, so that only the first or the second term on the R.H.S. of Eq. (34) contributes, respectively, to the corresponding NTQD deformation potentials [cf. Eqs. (30)-(33)]. Then, Eqs. (2), (4), (22), (23), (27)–(34) and

$$\nu = \pm 1 \quad \Rightarrow \quad \int_0^{2\pi} \frac{d\varphi}{2\pi} e^{\pm i\nu\varphi} \cos\varphi = \frac{1}{2}, \quad (35)$$

allow us to obtain

$$\begin{aligned} \langle \psi_{00\pm} | \hat{H}_{\text{X-ph}} | \psi_{00\pm} \rangle &\approx 2\nu g_2 (1 + \sigma) \cos 3\theta \langle F_{00} | \frac{\partial \hat{\phi}_c}{\partial z}(\hat{z}_e) | F_{00} \rangle + 2\xi R [g_1 (1 - \sigma) \\ &+ \nu \zeta g_2 (1 + \sigma) \cos 3\theta] \langle F_{00} | \frac{\partial^2 \hat{\phi}_f}{\partial z^2}(\hat{z}_e) E_{\perp}(\hat{z}_e) | F_{00} \rangle \end{aligned} \quad (36)$$

which is independent of the excitonic wavefunction's symmetry (bonding vs. antibonding). Here we have exploited the completeness of the basis  $\{|F_{-\nu 0, l}\rangle\}$ . The “off-diagonal” coupling to flexural phonons, i.e. the term proportional to  $\zeta$ , constitutes a negligible correction given that  $\zeta = \alpha_{FC} a_B / 3v_F R \lesssim 0.1$  (for stable CNT radii [52]) and  $g_2/g_1 \approx 0.05$ .

To recapitulate, in the present section we have used an envelope function approximation based on the graphene zone-folded description to analyse how weak inhomogeneous electrostatic fields affect the axially-polarised direct excitons of a wide-gap semiconducting CNT. We have shown that such perturbative fields can induce quantum confinement of the CM motion dominated by the axial component and characterised by a level spacing in the milli-electronvolt range, and have derived the effective deformation potential (DP) for the lowest-energy direct-exciton states of the resulting optically-active quantum dot (NTQD). This approximation for the excitonic DP in the presence of applied electrostatic fields, given by Eq. (36), constitutes a central result of this paper. It relies on: (i) the aforementioned envelope function approximation, (ii) the existence of a weakly confined Wannier-exciton state  $|\psi_{00}\rangle$  —which requires the adiabatic conditions on  $E_{\parallel}(z)$  detailed in Eq. (18), (iii) neglecting the dispersion of the relevant cross-polarised excitonic manifold and (iv) the weakness criterion on the transverse field  $|\xi E_{\perp}(z_0)|^2 \ll 1$  \*. This effective excitonic DP involves coupling to both compressional (i.e. stretching) and flexural phonons. The latter is linear in the transverse field  $E_{\perp}$  which induces a hybridisation with the cross-polarised excitons. Interestingly within our envelope function approximation (i), the 1D subband Bloch functions alternate between the two orthogonal eigenstates of the sublattice pseudospin  $\hat{\sigma}_{x'}$  as the corresponding eigenenergy is increased —cf. Eqs. (2) and (3). This leads to the selection rules embodied in Eqs. (24) and (25), which imply that the contribution from the  $E_{12}$  and  $E_{21}$  excitons vanishes.

\* Note that  $1/|\xi|$  is comparable to the transverse critical field for exciton dissociation —  $1/|\xi| \sim 10^4 \text{ V}\mu^{-1}$  for relevant nanotube parameters (cf. Sec. 3.1).

### 3. Exciton-assisted optomechanics

In this section we consider the scenario relevant for optomechanics where axial phonon-confinement due to the finite suspended-length of the CNT plays a leading role. Whence the flexural and compressional phonon branches of the CNT are characterised by sharp resonances with a free spectral range comparable to the optical linewidth of the zero phonon line (ZPL) of the transition associated to the state  $|\psi_{00-}\rangle$  (analogous considerations apply to  $|\psi_{00+}\rangle$ ). We focus on laser excitation of the latter near resonant with the ensuing lowest-frequency flexural phonon sidebands. More precisely, we consider a bridge geometry (cf. Fig. 1) with a length ( $L \sim 100$  nm) short enough that the relative strength of these phonon sidebands is weak, but long enough that phonon-radiation losses (i.e. clamping losses) are negligible [53]. Hereafter, we follow Ref. [32] in which an analogous scenario was analysed in a semiconductor heterostructure.

To this effect we use the formalism developed in Ref. [53] and adopt a resonator-bath representation with the resonator mode (annihilation operator  $b_0$ , angular frequency  $\omega_0$ , and quality factor  $Q$ ) corresponding to the fundamental in-plane flexural resonance (that we intend to manipulate and laser cool to the ground state) and the bath including the other nanotube vibrational resonances coupled to the 3D substrate that supports the CNT. Thus, we use for the effective field operators  $\hat{\phi}_f$ ,  $\hat{\phi}_c$  in Eq. (36) the following resonator-bath mode decomposition

$$\begin{aligned} \frac{\partial^2 \hat{\phi}_f}{\partial z^2}(\hat{z}_e) &\rightarrow \frac{\partial^2 \phi_0}{\partial z^2}(\hat{z}_e) \sqrt{\frac{\hbar}{2\mu\omega_0}} b_0 + \sum_q \frac{\partial^2 u_{x,q}}{\partial z^2}(\hat{z}_e) \sqrt{\frac{\hbar}{2\rho_s\omega(q)}} b_q + \text{H.c.}, \\ \frac{\partial \hat{\phi}_c}{\partial z}(\hat{z}_e) &\rightarrow \sum_q \frac{\partial u_{z,q}}{\partial z}(\hat{z}_e) \sqrt{\frac{\hbar}{2\rho_s\omega(q)}} b_q + \text{H.c.} \end{aligned} \quad (37)$$

Here  $\phi_0(z)$  is the normalised resonator 1D eigenmode and  $\mu$  is the linear mass density of the CNT; while  $u_{x,q}(z)$  [ $u_{z,q}(z)$ ] with  $z \in \text{CNT}$  is the  $x$  [ $z$ ] component of the centre of mass displacement of the CNT cross section at  $z$  (cf. Fig. 1) for the bath mode (annihilation operator  $b_q$ ) corresponding to the scattering eigenmode  $q$  [53], and  $\rho_s$  is the mass density of the substrate. Subsequently, substituting Eq. (37) into Eq. (36) we obtain

$$|\psi_{00\pm}\rangle \langle \psi_{00\pm}| \hat{H}_{\text{X-ph}} |\psi_{00\pm}\rangle \langle \psi_{00\pm}| = \hbar \left( \eta \omega_0 b_0 + \sum_q \lambda_q b_q + \text{H.c.} \right) |\psi_{00\pm}\rangle \langle \psi_{00\pm}| \quad (38)$$

with

$$\begin{aligned} \lambda_q \approx & \sqrt{\frac{\hbar}{2\rho_s\omega(q)}} \left\{ 2\nu g_2 (1 + \sigma) \cos 3\theta \langle F_{00} | \frac{\partial u_{z,q}}{\partial z}(\hat{z}_e) | F_{00} \rangle \right. \\ & \left. + 2\xi R g_1 (1 - \sigma) \langle F_{00} | \frac{\partial^2 u_{x,q}}{\partial z^2}(\hat{z}_e) E_{\perp}(\hat{z}_e) | F_{00} \rangle \right\} \end{aligned} \quad (39)$$

and

$$\eta \approx 2^{3/4} (1 - \sigma) \frac{g_1 \sigma_G^{1/4} \xi \mathcal{E}_{\perp}}{R E_G^{3/4} (q_0 L)} \sqrt{\frac{L}{\pi \hbar}}, \quad (40)$$

where we have introduced the effective field  $\mathcal{E}_\perp \equiv (\sqrt{L}/q_0^2)\langle F_{00}|\frac{\partial^2\phi_0}{\partial z^2}(\hat{z}_e)E_\perp(\hat{z}_e)|F_{00}\rangle$ , set  $\zeta \rightarrow 0$  and used  $\omega_0 = \tilde{c}_c R q_0^2/\sqrt{2}$ . Here  $q_0 \approx 4.73/L$  is the fundamental mode's Euler-Bernoulli wavevector for clamped-clamped boundary conditions, and  $E_G = 340 \text{ Nm}^{-1}$  and  $\sigma_G = 7.6 \times 10^{-7} \text{ kgm}^{-2}$  are, respectively, the 2D Young modulus [54] and mass density of graphene ( $a = 0.246 \text{ nm}$  [50]). The parameter  $\eta$  is the ‘‘modulation parameter’’ associated to the phonon sidebands that characterises the strength of the exciton-resonator coupling with  $e^{-\eta^2/2}$  corresponding to the Franck-Condon factor ( $\eta^2$  is also known as the Huang Rhys parameter). We will focus mainly on regimes such that  $\eta \ll 1$ . Note that the perturbative nature of  $E_\perp$  underpinning Eq. (40) implies  $\xi\mathcal{E}_\perp \ll 1$ .

Then from Eq. (38), adopting Pauli matrix notation for the optical pseudospin ( $\sigma_z = 1$  corresponds to  $|\psi_{00-}\rangle$  and  $\sigma_z = -1$  to the empty neutral NTQD) and a frame rotating at the laser frequency  $\omega_L$ , and applying the shift

$$\hat{O}' = e^{-\frac{\eta}{2}(b_0 - b_0^\dagger) - \sum_q \frac{\lambda_q}{2\omega_q}(b_q - b_q^\dagger)} \hat{O} e^{\frac{\eta}{2}(b_0 - b_0^\dagger) + \sum_q \frac{\lambda_q}{2\omega_q}(b_q - b_q^\dagger)} \quad (41)$$

to the phonon modes, we obtain the following Hamiltonian for the laser driven NTQD coupled to the resonator mode ( $\hbar = 1$ )

$$H'_{\text{sys}} = -\frac{\delta}{2}\sigma_z + \frac{\Omega}{2}\sigma_x + \frac{\eta\omega_0}{2}\sigma_z (b_0 + b_0^\dagger) + \omega_0 b_0^\dagger b_0. \quad (42)$$

Here  $\delta$  is the laser detuning from the ZPL and  $\Omega$  the Rabi frequency.

To analyse the dynamics that arises from the interplay between  $H'_{\text{sys}}$  and the couplings to the phonon bath and to the radiation field (annihilation operators  $a_k$  and couplings  $g_k$ ), we perform the following canonical transformation [32]

$$\hat{O}' = e^{-\frac{\eta}{2}\sigma_z(b_0 - b_0^\dagger)} \hat{O} e^{\frac{\eta}{2}\sigma_z(b_0 - b_0^\dagger)} \quad (43)$$

to a ‘‘polaronic’’ representation. The resulting complete Hamiltonian consists of three contributions,  $H = H_{\text{sys}} + H_{\text{int}} + H_B$ , given by ( $\hbar = 1$ )

$$H_{\text{sys}} = -\frac{\delta}{2}\sigma_z + \frac{\Omega}{2}(\sigma_+ B^\dagger + \sigma_- B) + \omega_0 b_0^\dagger b_0 \quad (44)$$

$$H_{\text{int}} = \sum_k g_k \sigma_+ B^\dagger a_k + \sum_q \zeta_q b_0^\dagger b_q + \frac{\sigma_z}{2} \sum_q \lambda_q b_q + \text{H.c.} \quad (45)$$

$$H_B = \sum_q \omega_q b_q^\dagger b_q + \sum_k (\omega_k - \omega_L) a_k^\dagger a_k, \quad (46)$$

where  $B \equiv e^{\eta(b_0 - b_0^\dagger)}$ . The couplings  $\zeta_q$  and  $\lambda_q$  to the phonon bath lead, respectively, to the resonator-mode's phonon-radiation losses and to pure dephasing of the NTQD induced by the deformation potential [cf. Eqs. (38) and (39)]. To assess their role we note that: (i)  $qR \ll 1$  and (ii) the reflection symmetry of the whole structure with respect to the  $y - z$  plane, imply that the  $q$  can be effectively identified with the low-frequency CNT phonon branches so that the couplings  $\zeta_q$  involve only modes with a flexural character [53]. The RWA for the latter is justified given  $Q \gg 1$  and  $\eta \ll 1$ . These conditions and the anharmonicity of the flexural spectrum also imply that the effects of the  $\lambda_q$  associated to the flexural branch can be neglected [55].

In turn, the pure dephasing induced by the compressional (stretching) phonons is determined by the low-frequency behaviour of the spectral density

$$J_c(\omega) = \pi \sum_q |\lambda_q|^2 \delta(\omega - \omega_q) \quad (47)$$

with  $q \in$  compressional branch. The latter can be obtained from Eq. (39), building upon the scattering formalism previously developed (cf. Eq. (34) in Ref. [53]) by incorporating now the leading correction in  $qR$  to the zeroth order 1D-3D reflection amplitude at a single junction between the resonator and the support (clamping point) and considering the “single support” case in which both clamping points connect to the same elastic half-space so that interference effects are crucial — as relevant to our scenario where the gap below the CNT satisfies  $\lesssim L$  (cf. Fig. 1). This procedure which will be detailed elsewhere yields a superohmic phonon spectral density [56],

$$J_c(\omega) \approx 2\pi\alpha_{\text{con}} \frac{\omega^3}{\omega_*^2} \quad \text{for} \quad \omega \ll \omega_*, \quad (48)$$

with

$$\alpha_{\text{con}} \sim \frac{\alpha}{\pi Q_c} \quad \text{and} \quad \omega_* \sim \frac{c_{\text{SAW}}}{L}, \quad (49)$$

where

$$Q_c = \frac{0.22}{\pi^2} \sqrt{\frac{\sigma_G}{\rho_s} \left(\frac{E_s}{E_G}\right)^3} \frac{L^2}{R} \quad (50)$$

is the clamping-loss limited  $Q$ -value of the fundamental compressional mode for the “double support” case [53] ( $Q_c \sim 50$  for  $L \sim 100$  nm), and  $\alpha$  is the dimensionless dissipation parameter [56] for the corresponding Ohmic (1D continuum) result (note that the size of the QD-molecule generated by the tip electrodes is set by  $z_0$ )

$$J_c(\omega) = 2\pi\alpha\omega \quad \text{for} \quad \omega \ll \omega_U \sim \tilde{c}_c/z_0 \quad (51)$$

which is valid in the limit  $L \rightarrow \infty$  (keeping  $\omega$  fixed). Here  $c_{\text{SAW}}$  and  $E_s$  are, respectively, the phase velocity of surface acoustic waves and Young modulus of the substrate which is assumed to have a Poisson ratio  $\nu_s = 1/3$ .

The dissipation parameter  $\alpha$  plays a crucial role in determining the different phases of the corresponding spin-boson model [Eqs. (44)-(46) with  $\eta = g_k = \zeta_q = 0$ ] in particular whether excitonic Rabi oscillations are possible for  $\Gamma \ll \Omega < \omega_U$  [56]. Using the results of Sec. 2.2 it is straightforward to obtain

$$\alpha = \frac{g_2^2 \sqrt{\sigma_G} (1 + \sigma)^2}{2\pi^2 \hbar R E_G^{3/2}} \cos^2 3\theta \quad (52)$$

which has a marked dependence on the chirality angle  $\theta$ . We note that for stable CNT radii Eq. (52) always yields  $\alpha < 0.02$ . In turn, a straightforward analysis of the linear absorption spectrum (i.e. for  $\Omega \ll \Gamma$ ) that results from this weak-coupling continuum Ohmic model [56] (in the relevant low temperature regime  $k_B T/\hbar \ll \omega_U$ ) implies a pure-dephasing contribution to the linewidth given by  $\gamma_{\text{ph}} = 2\pi\alpha k_B T/\hbar$  and an asymmetric

power law tail  $\sim \delta^{2\alpha-1}$  which is only observable for  $\max\{\Gamma, \gamma_{\text{ph}}\} \ll 2^{-1/2\alpha}$ . The confined scenario embodied by Eq. (48) leads to a favourable suppression of this phonon-induced decoherence which would otherwise preclude achieving the desired resolved-sideband condition for realistic parameters (cf. Sec. 3.1). Thus, this feature constitutes a cornerstone for the scheme proposed here. More precisely, the superohmic behaviour with  $n \geq 3$  and  $\alpha_{\text{con}} \ll 1$  implies that for relevant ratios  $\Gamma/\omega_0$  and  $\Omega \lesssim \omega_0$  (cf. 3.1), the impact of these “background modes” on optomechanical effects involving the resonator mode is completely negligible [55] — henceforth we take  $\lambda_q \rightarrow 0$ .

In the following subsections we show how the resulting optomechanical system can be used for ground-state cooling of the fundamental mode (Sec. 3.1), consider the main practical limits to the strength of the optomechanical coupling that can be achieved (Sec. 3.2), and discuss the prospects for reaching the corresponding strong and ultra-strong coupling regimes (Sec. 3.3).

### 3.1. Laser-cooling

To analyse laser cooling of the resonator mode we derive, first, a reduced master equation for the NTQD-resonator system and, subsequently, a rate equation for its populations. For the relevant regimes all environmental couplings can be treated within the Born-Markov approximation and, after eliminating the bath phonon modes and the radiation field, the Liouvillian of the driven NTQD coupled to the resonator mode reads

$$\begin{aligned} \dot{\rho} = & -i[H_{\text{sys}}, \rho] + \frac{\Gamma}{2}(2\sigma_- B \rho B^\dagger \sigma_+ - \rho \sigma_+ \sigma_- - \sigma_+ \sigma_- \rho) \\ & + \omega_0 \frac{n(\omega_0)}{2Q} \left( 2b_0^\dagger \rho b_0 - b_0 b_0^\dagger \rho - \rho b_0 b_0^\dagger \right) \\ & + \omega_0 \frac{n(\omega_0)+1}{2Q} \left( 2b_0 \rho b_0^\dagger - b_0^\dagger b_0 \rho - \rho b_0^\dagger b_0 \right), \end{aligned} \quad (53)$$

where  $n(\omega_0)$  is the thermal equilibrium occupancy at the ambient temperature,

$$\Gamma = 2\pi \sum_k |g_k|^2 \delta(\omega_L - \delta - \omega_k) \quad \text{and} \quad \frac{\omega_0}{Q} = 2\pi \sum_q |\zeta_q|^2 \delta(\omega_0 - \omega_q). \quad (54)$$

Other relevant sources of dissipation beyond those considered in Hamiltonian Eqs. (44)-(46); namely, internal losses of the CNT resonator and nonradiative recombination of the exciton [24] can be incorporated, respectively, by simply adopting modified values of  $Q$  and  $\Gamma$ . We note that the nonradiative recombination rate for an ultra-clean CNT dark exciton has not been measured so far.

In analogy with the Lamb-Dicke limit (LD approximation) we expand up to second order the translation operators  $B$  and adiabatically eliminate the NTQD to obtain a rate equation for the populations of the resonator mode’s Fock states [57]. The latter reads [32]

$$\begin{aligned} \dot{P}_n = & \left[ \eta^2 A_+ + \omega_0 \frac{n(\omega_0)}{Q} \right] [nP_{n-1} - (n+1)P_n] + \left[ \eta^2 A_- + \omega_0 \frac{n(\omega_0)+1}{Q} \right] \\ & \times [(n+1)P_{n+1} - nP_n] \end{aligned} \quad (55)$$

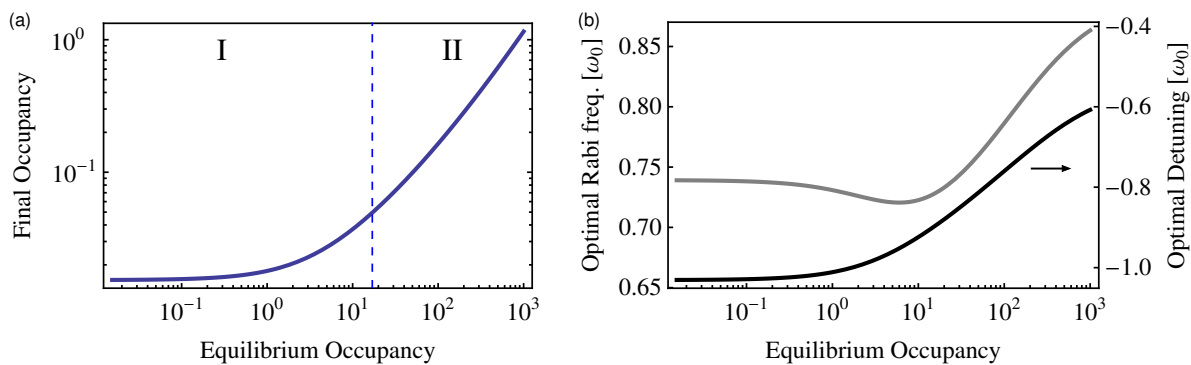


**Figure 2.** (a) Optimal steady state (final) occupancy ( $n_f$ ) v.s. equilibrium (thermal) occupancy  $n(\omega_0)$  for  $\Gamma/\omega_0 = 1/2$  and  $\eta^2 Q = 1.1 \times 10^3$ . The optimum results from minimising  $n_f$  with respect to the laser parameters. For  $n(\omega_0) \leq (\frac{\Gamma}{4\omega_0})^2$  laser cooling is not operational. For  $n(\omega_0) \geq (\frac{\Gamma}{4\omega_0})^2$  there are two regimes (dotted line): I) when  $n(\omega_0) \ll \eta^2 Q (\frac{\Gamma}{4\omega_0})^2$ ,  $n_f$  is determined by the quantum backaction limit  $\approx (\frac{\Gamma}{4\omega_0})^2$  and II) when  $n(\omega_0)$  is large [ $n(\omega_0) \gg \eta^2 Q (\frac{\Gamma}{4\omega_0})^2$ ] thermal noise dominates and the optimum becomes linear in the ambient temperature. (b) Rabi frequency (gray) and laser detuning (black) for which  $n_f$  is minimised (in units of  $\omega_0$ ).

with the cooling ( $\eta^2 A_-$ ) and heating ( $\eta^2 A_+$ ) transition rates per quanta determined by  $A_{\mp} = \Gamma[(\delta \mp \omega_0)^2 + \Gamma^2/4](\omega_0^2 + \Gamma^2 + \Omega^2/2)\Omega^2/D$ , where

$$D \equiv 4 \left( \delta^2 + \frac{\Gamma^2}{4} + \frac{\Omega^2}{2} \right) \left\{ (\omega_0^2 + \Gamma^2) \left[ (\delta - \omega_0)^2 + \frac{\Gamma^2}{4} \right] \left[ (\delta + \omega_0)^2 + \frac{\Gamma^2}{4} \right] + \left[ \delta^2 (2\omega_0^2 + \Gamma^2) - (2\omega_0^2 - \Gamma^2) \left( \omega_0^2 + \frac{\Gamma^2}{4} \right) \right] \Omega^2 + \left( \omega_0^2 + \frac{\Gamma^2}{4} \right) \Omega^4 \right\}. \quad (56)$$

We note that in this system, in stark contrast to atomic laser cooling,  $A_{\mp} \rightarrow 0$  in the limit  $\Omega \rightarrow \infty$  — in the polaronic representation this is associated to quantum interference effects between multiple paths[32]. Thus the steady state occupancy for  $Q \rightarrow \infty$ , i.e. the quantum backaction limit, reduces to

$$\frac{A_+}{A_- - A_+} = -\frac{(\delta + \omega_0)^2 + \frac{\Gamma^2}{4}}{4\delta}. \quad (57)$$

Remarkably, this result is independent of the Rabi frequency and coincides with the expression valid for the optomechanical cavity-assisted backaction cooling [58, 59] (Eq. (6) in Ref. [58]) with the cavity decay rate  $1/\tau$  replaced by the spontaneous emission rate which for the optimal detuning  $\delta = -\sqrt{\omega_0^2 + \Gamma^2/4}$  yields the fundamental limit  $(\sqrt{1 + (\Gamma/2\omega_0)^2} - 1)/2$ . This coincidence can be better understood by performing the adiabatic elimination in the “original” representation corresponding to Eq. (42) — a thorough analysis using this representation has been performed by Jaehne et al. [60].

Figure 2 shows the resulting temperature dependence of the optimal steady state occupancy ( $n_f$ ) that follows from Eq. (55), i.e.

$$\langle b_0^\dagger b_0 \rangle_{\text{ss}} = \frac{n(\omega_0) + \eta^2 Q A_+ / \omega_0}{1 + \eta^2 Q (A_- - A_+) / \omega_0} \quad (58)$$

minimised with respect to the laser detuning  $\delta$  and Rabi frequency  $\Omega$ , for typical parameters. These correspond for instance to  $\Gamma = \omega_0/2$ ,  $Q = 1.5 \times 10^5$  and  $\eta = 0.086$ . The latter can be realised for example with a (9, 4) nanotube [cf. Eq. (40)] ‡ ( $R = 0.45\text{nm}$ ) of length  $L = 120\text{ nm}$  ( $\omega_0/2\pi = 1.67\text{ GHz}$ ) and a transverse effective field  $\mathcal{E}_\perp = 36.8\text{ V}\mu^{-1}$  (corresponding to the field configuration in Fig. 1). For this case an ambient temperature  $T = 4.2\text{ K}$  [ $n(\omega_0) = 52$ ] allows cooling to a final (steady state) occupancy  $n_f = 0.10$ . In the high temperature regime (II) the cooling factor is constant and straightforward arguments imply that its optimum is approximately bounded by  $\eta^2 Q \lesssim n(\omega_0)/n_f \lesssim \eta Q$  [32, 60]. We note that for the parameters considered here (cf. Fig. 1) in this linear regime the initial effective modulation parameter is no longer small, i.e.  $\eta^2[n(\omega_0) + 1] \gtrsim 1$  and we find for the optimum  $A_-|_{\text{opt}} \sim (A_- - A_+)|_{\text{opt}} \sim \omega_0$ , so that initially  $\eta^2[\langle b_0^\dagger b_0 \rangle + 1]A_- \gtrsim \Gamma$  and Eq. (56) fails to describe the complete cooling process which will suffer a slowing down. Nonetheless for these parameters  $\eta^2[n_f + 1]A_-|_{\text{opt}}/\Gamma < 0.03$  for all  $n(\omega_0) < 10^3$ , and the LD approximation remains valid for the steady state — these aspects have been analysed in detail by Rabl [62].

### 3.2. Implementation

The choice of parameters in section 3.1 takes into account the restrictions imposed on the applied electric fields by the need to avoid: deleterious static deflections due to gradient forces [63], field emission, and dielectric breakdown (cf. Fig. 1). For the nanotube the latter is taken care of by the aforementioned restrictions imposed on the fields  $E_\perp(z_0) \sim E_\perp(0)$  and  $E_\parallel(z_0)$  so as to avoid dissociation of the  $E_{11}$  exciton (cf. Sec. 2), while the suspended tip geometry of the electrodes (cf. Fig. 1) allows for a strong suppression of the field at the dielectric substrate with respect to the maximum field. In fact, static deflections pose the most stringent limitation when trying to maximise the exciton-resonator coupling  $\eta$ , given that they scale as

$$\Delta x \sim \frac{(\alpha_\parallel + \alpha_\perp)}{\pi^5 E_G} \left(\frac{L}{R}\right)^3 E_\perp(0)E_\parallel(z_0) \quad (59)$$

—here the prefactor is of order unity provided that the transverse dimension of the electrodes is comparable to or smaller than  $z_0 < L$ , and we have used the reflection symmetries which imply that the total electrostatic force on the nanotube scales as  $2(\alpha_\parallel + \alpha_\perp)E_\perp(0)E_\parallel(z_0)$ . Note that due to the Duffing geometric nonlinearity associated to a bridge geometry this static deflection would result mainly in an effective stiffening of the resonator for  $\Delta x \gtrsim R$ . For the parameters considered in Sec. 3.1, a detailed calculation based on the FEM electric fields (cf. Sec. 2.1), the Euler-Bernoulli theory for the CNT flexural response, and static polarisabilities [ $\alpha_\perp = 13(4\pi\epsilon_0\text{\AA}^2)$ ,  $\alpha_\parallel = 75(4\pi\epsilon_0\text{\AA}^2)$ ] estimated from Refs. [64, 65] yields  $\Delta x = 0.013\text{ nm}$  (note  $R = 0.45\text{nm}$ ).

‡ Since to our knowledge the optical transition energy  $E_{13}$  has so far not been determined, we take as a rough estimate for the energy difference in  $\xi$ ,  $E_{13} - E_{11} \sim E_{12} + 2\hbar v_F/3R$  which corresponds to assuming that the correlation energy for  $E_{13}$  is the same as for the cross-polarised excitons  $E_{12}$ , and use for the latter the value reported in Ref. [61] — this procedure yields 1.3 eV.

Under these conditions we find that the modification of the resonator's frequency  $\omega_0 \rightarrow \tilde{\omega}_0$  induced by the electric fields and the effect of the Duffing geometric nonlinearity (which lead, respectively, to softening and stiffening) is completely negligible ( $\sim 0.1\%$ ). In general, this modification also results in a correction to the NTQD modulation parameter given by  $\eta \rightarrow (\omega_0/\tilde{\omega}_0)^{3/2}\eta$ .

The proposed device is compatible with a confocal setup but places stringent requirements on the nanotube positioning needed to enforce the desired reflection symmetries. We note that the latter are not essential to our scheme but just a convenient means to enable a wider parameter range. If they are relaxed, while it is still possible to tune independently  $\Delta E$  and  $\eta$  via the two voltages  $V_1$  and  $V_2$ ,  $|V_2 - V_1| \gg |V_2 + V_1|$  can now result in regions where  $E_\perp \sim E_\parallel$  which reduces the maximum feasible  $E_\perp$  given that  $E_\parallel$  should not exceed the critical field for the breakdown of an  $E_{11}$  exciton. Nonetheless, relevant couplings could still be achieved [cf. Eq. (40)]. In turn for such an asymmetric arrangement the NTQD may also couple to the out-of-plane flexural resonances but this has no impact on the validity of our effective model [Eqs. (44)-(46) with  $\lambda_q = 0$  for  $q \in$  flexural branch] given that the electrostatic fields and the mechanical coupling to the substrate break the degeneracy between the two flexural branches. A variant of this asymmetric scenario, albeit relinquishing the independent tunability of  $\Delta E$  and  $\eta$ , is to use a single voltage configuration in which the fields are applied with an STM tip. Another interesting option is to effect the optical excitation of the nanotube using the evanescent field of a tapered fibre which could allow for instance to cancel the static deflection by using the optical gradient forces induced by an additional off-resonant laser, thereby lifting the restriction imposed on the length by Eq. (59) [66].

As the required fields are relatively large ( $\sim 10\text{V}\mu^{-1}$ ) and inhomogeneous, it seems natural to also analyse the impact of voltage fluctuations arising from the Johnson-Nyquist noise of the electrodes and/or of the voltage sources used. These induce a fluctuation of the effective potential defining the NTQD [cf. Eq. (11)]

$$\delta\hat{V}_{\text{eff}}^{(V)}(\hat{z}_{\text{CM}}) = -2\alpha_X^{(00)} \frac{E_\parallel^2(\hat{z}_{\text{CM}})}{V_1 + V_2} \left( \delta\hat{V}_1 + \delta\hat{V}_2 \right) \quad (60)$$

which given  $k_B T < \Delta E$ , only affects the exciton as a pure dephasing contribution described by the interaction Hamiltonian  $H_p = \frac{1}{2}\sigma_z \hat{V}_p$  with  $\hat{V}_p = \langle F_{00} | \delta\hat{V}_{\text{eff}}^{(V)}(\hat{z}_{\text{CM}}) | F_{00} \rangle$ . Here the white noise variables  $\delta\hat{V}_1$  and  $\delta\hat{V}_2$  are uncorrelated and determined by  $\langle \delta\hat{V}_{1/2}(t) \delta\hat{V}_{1/2}(0) \rangle = 2R_J k_B T \delta(t)$  where  $R_J$  and  $T$  are the relevant resistance and temperature —for estimating an upper bound we assume without loss of generality that the noise is symmetric and dominated either by the electrodes or the unfiltered sources. Then within the Markov approximation, these voltage fluctuations result in an excess linewidth (FWHM)  $\gamma_p = \int_{-\infty}^{\infty} \langle \hat{V}_p(t) \hat{V}_p(0) \rangle dt / \hbar^2$ . The latter can be estimated using Eqs. (60), (14) and  $\langle F_{00} | E_\parallel^2(\hat{z}_{\text{CM}}) | F_{00} \rangle \sim E_\parallel^2(z_0)$  leading to

$$\gamma_p \sim R_J k_B T \left[ \frac{32\pi\epsilon_0\epsilon_\parallel}{\hbar(V_1 + V_2)} \right]^2 \sigma_{eh}^6 E_\parallel^4. \quad (61)$$

Finally, for the envisaged parameters (cf. Sec. 2.1 and Fig. 1),  $R_J < 1\Omega$  and  $T < 300\text{ K}$ , Eq. (61) yields  $\gamma_p/2\pi \lesssim 200\text{ kHz}$  which is negligible compared to the values for  $\Gamma \gtrsim 100\text{ MHz}$  considered here (cf. Secs. 3.1 and 3.3). In principle, this voltage noise will also induce a fluctuation of the gradient forces exerted on the CNT [cf. Eq. (59)] resulting in additional dissipation of the resonator mode. However this effect is completely negligible for relevant parameters  $\dagger\dagger$ .

Another potential source of exciton dephasing is the Brownian motion of the suspended portion of the electrodes which entails a limit to the suspended length, beyond which performance would be degraded. The convenience of electrode suspension, beyond that imposed by fabrication constraints, resides in the suppression it can induce of the maximum electric field at the neighbouring dielectric free surfaces ( $E_{\text{d-f}}$ ) with respect to the maximum field. Assuming a cantilever geometry for the suspended portion of the electrode and an electrode-substrate gap size comparable to the suspended length  $L_e$ , the suppression factor will scale as  $(h_e/2L_e)^2$  —where  $h_e$  is the transverse dimension of the electrode. For the envisaged device (cf. Fig. 1)  $h_e = 30\text{ nm}$  and  $L_e = 100\text{ nm}$  would already lead to  $E_{\text{d-f}} \lesssim 5\text{ V}\mu^{-1}$ . If we assume some generic misalignment of the CNT, both the Brownian motion of the electrode's flexural (in-plane and/or out-of-plane) and compressional modes will contribute a term linear in the relevant displacement  $X_e$  to the corresponding fluctuation of the effective confining potential  $\delta\hat{V}_{\text{eff}}^{(B)}$ . The latter will play a role completely analogous to  $\delta\hat{V}_{\text{eff}}^{(V)}$  but with  $\delta\hat{V}_{1/2}$  replaced by the  $\{X_e\}$ . In all cases the relevant fluctuation of the electric field satisfies

$$\delta E_{\parallel}(z_0) \lesssim \frac{E_{\parallel}(z_0)}{z_0} X_e \quad (62)$$

and a suitable model to estimate an upper bound for the corresponding excess linewidth (FWHM)  $\gamma_B$  is afforded by considering only the contributions from the fundamental resonances of each relevant branch (resonant frequency  $\omega_e$ ) which can be treated separately —we assume in what follows that the Brownian motions of different electrodes are uncorrelated. These contributions can be analysed using the exact solution of the ensuing independent-boson model [55]. If we assume Au electrodes with the aforementioned cantilever dimensions, we have for the fundamental flexural mode  $\omega_e \sim 1\text{ GHz}$  so that  $\Gamma \lesssim \omega_e$  (cf. Secs. 3.1 and 3.3). There are then two distinct effects of the electrodes' Brownian motion on the optical response of the exciton that could potentially interfere with our scheme: (i) generation of a sideband spectrum and (ii) pure dephasing leading to an excess linewidth of the corresponding ZPL. A critical parameter is the relative weight of the single-phonon sidebands ( $S$ ) which for each branch, in the relevant regime  $k_B T \gg \hbar\omega_e$  and using Eqs. (11) and (62), can be bounded by

$$S_e \lesssim k_B T \left( \frac{16\pi\epsilon_0\epsilon_{\parallel}}{\hbar z_0} \right)^2 \frac{\sigma_{eh}^6 E_{\parallel}^4}{m_e \omega_e^4} \quad (63)$$

$\dagger\dagger$  A straightforward derivation using that the susceptibility associated to the voltage noise is determined by  $\Im\{\chi(\omega)\} = R_J\omega$ , yields for the corresponding contribution to the mechanical linewidth  $\gamma_m \sim \frac{8R_J(V_2^2+V_1^2)}{\pi\sigma_G RL(V_2^2-V_1^2)^2}(\alpha_{\parallel} + \alpha_{\perp})^2 E_{\perp}(0)^2 E_{\parallel}(z_0)^2$  which for  $R_J < 1\Omega$  implies  $\gamma_m/2\pi \lesssim 50\text{ }\mu\text{Hz}$ .

where  $m_e$  is the corresponding effective mass. If we consider the envisaged device parameters (cf. Sec. 2.1 and Fig. 1), the aforementioned “electrode” cantilever dimensions, the material properties of Au and  $T = 4.2$  K, we obtain from Eq. (63) adding over all relevant branches of both electrodes;  $S \lesssim 0.07$  —the ratio of the corresponding polaron shift to the one associated to the CNT resonator ( $\eta^2\omega_0$ ) is  $\lesssim 0.03$  (cf. Sec. 3.1). Thus, the influence of (i) on the proposed optomechanical manipulations would be minimal.

In turn, the pure dephasing (ii) is determined by the weak dissipation of these resonances induced by the 3D substrate and is characterised by an Ohmic environmental spectral density. The conditions  $S \ll 1$  and  $k_B T \gg \hbar\omega_e$  are sufficient to ensure that the dephasing is Markovian and amenable to a treatment similar to the one we have followed for the voltage fluctuations. Each of the relevant fundamental resonances coupled to the substrate satisfies [53]

$$\int_{-\infty}^{\infty} \langle X_e(t) X_e(0) \rangle dt = \left( \frac{2x_e^{(0)}}{\omega_e} \right)^2 \frac{k_B T}{\hbar Q_e} \quad (64)$$

where  $x_e^{(0)}$  and  $Q_e$  are, respectively, the corresponding zero-point motion and  $Q$ -value. Then, following a procedure analogous to the one used for estimating  $\gamma_p$ , we obtain from Eqs. (11), (62) and (64)

$$\frac{\gamma_B}{2\pi} \lesssim k_B T \frac{\sqrt{\rho_s}}{E_s^{3/2}} \left( \frac{16\pi\epsilon_0\epsilon_{\parallel}}{\hbar z_0} \right)^2 \sigma_{eh}^6 E_{\parallel}^4. \quad (65)$$

Here we have also assumed that given the low aspect ratio, the  $\{Q_e\}$  are limited by clamping losses, used the results of Ref. [53] (Table I) which imply that  $m_v Q_v \omega_v^3 = m_h Q_h \omega_h^3 \sim m_c Q_c \omega_c^3 \sim E_s^{3/2} / \sqrt{\rho_s}$ , and added the bounds for all three relevant branches of both electrodes —here  $v$ ,  $h$  and  $c$  label, respectively, the flexural vertical, flexural horizontal and compressional fundamental resonances of the “electrode” cantilever and the dimensionless prefactors are functions of  $\nu_s$ . Strikingly once a cantilever geometry is assumed, the dimensionless prefactor close to unity in Eq. (65) is independent of any other property of the electrode as it only depends on the Poisson ratio of the substrate. Thus, the magnitude of the suspended length  $L_e$  would only begin to play a role in exciton dephasing if it became large enough to ensure that the mechanical dissipation were dominated by internal losses. Finally, we find that for the proposed parameters (cf. Sec. 2.1 and Fig. 1) and typical substrate properties determined by  $\rho_s = 2 \text{ gcm}^{-3}$  and  $E_s = 100 \text{ GPa}$ , Eq. (65) yields a completely negligible excess linewidth  $\gamma_B/2\pi \lesssim 20 \text{ kHz} \ll \Gamma$ .

Lastly, we have estimated radiation pressure effects and found that the corresponding static deflection and shot noise heating rate are also completely negligible, with typical parameters implying a launched power for a diffraction-limited spot size below 1 nW.

### 3.3. Strong coupling

Beyond optical transduction and cooling, the platform introduced here could allow us to realise a mechanical analogue of the strong and ultra-strong coupling regimes of cavity QED. If the driving laser is tuned exactly on resonance, i.e.  $\delta = 0$  in Eq. (42), after a  $\pi/2$  rotation of the pseudospin around  $\hat{y}$  ( $\sigma_z \rightarrow \sigma_x$ ,  $\sigma_x \rightarrow -\sigma_z$ ), the system Hamiltonian reduces to the Rabi model [67] ( $H'_{\text{sys}} \rightarrow H''_{\text{sys}}$ )

$$H''_{\text{sys}} = -\frac{\Omega}{2}\sigma_z + \frac{\eta\omega_0}{2}\sigma_x (b_0 + b_0^\dagger) + \omega_0 b_0^\dagger b_0 \quad (66)$$

with the spin degree of freedom afforded by the NTQD states dressed by the laser field, i.e.

$$|\pm\rangle' = \frac{1}{\sqrt{2}} (|\uparrow\rangle' \pm |\downarrow\rangle') \rightarrow |\downarrow / \uparrow\rangle'' . \quad (67)$$

Here  $|\uparrow\rangle' \equiv |\psi_{00-}\rangle$  corresponds to the relevant single-exciton state and  $|\downarrow\rangle'$  to the empty NTQD. The spin-oscillator coupling and resonance condition are given, respectively, by  $\eta\omega_0/2$  and  $\Omega = \omega_0$ . Thus, given  $1/Q \ll \eta \ll 1$  reaching the strong coupling regime of the Jaynes-Cummings model (i.e. the Rabi model neglecting counter-rotating terms) depends on satisfying  $\eta\omega_0 \gtrsim \Gamma$ , which for the aforementioned parameters would require  $\Gamma/2\pi \lesssim 100$  MHz. Here the precise threshold will differ from the more usual one,  $\eta\omega_0 = \Gamma/2$ , given that the dissipation of the pseudospin induced by the radiation will no longer correspond to a simple relaxation channel. As discussed in Sec. 2 the radiative contribution to  $\Gamma$  can be tuned with the axial magnetic field. We note that as the bright-dark exciton splitting lies in the 100 GHz range (cf. Sec. 2) and the radiative decay rate of the bright exciton is in the 10 GHz range [23],  $\Gamma \sim 100$  MHz with  $\Omega \sim \omega_0 \sim 1$  GHz is compatible with keeping the excitation of the bright exciton off-resonant.

The strong coupling regime discussed here is akin to the ion-trap realisations of the Jaynes-Cummings model and the parametric normal mode splitting in cavity optomechanics [68] in that the large energy-scale discrepancy between the optical and mechanical domains is bridged by the driving laser which entails an advantageous frequency-upconversion of the output. It offers a wide range of possibilities for the demonstration of quantum signatures in the motion. In particular a judicious modulation of  $\eta$  locked to pulsed laser excitation could allow us to emulate the adiabatic passage scheme used in Ref. [34] for performing QND measurements of the oscillator's energy. This would enable the observation of motional quantum jumps.

Furthermore, from the analysis in Sec. 3.2 it follows that higher transverse fields  $\mathcal{E}_\perp$  could be applied without disrupting the scheme. Then, a ten-fold increase in  $\mathcal{E}_\perp$  would result in  $\eta \sim 1$  allowing to crossover to the ultra-strong coupling regime of the Rabi model which has not been realised so far [67]. In this regime where the coupling becomes comparable with or larger than the resonator's level spacing, the ground state is characterised by an appreciable mean phonon occupancy and presents substantial entanglement between the excitonic quantum dot and the resonator [69]. To gain insight into this regime it is instructive to consider the limit  $\eta \gg 1$  which is simple to analyse

in the “polaronic” representation by treating the second term in the L.H.S. of Eq. (44) perturbatively. Thus, one obtains for the ground state of the coupled system

$$|\phi_0\rangle = \frac{1}{2} [ |+\rangle' (|+\alpha\rangle + |-\alpha\rangle) + |-\rangle' (|+\alpha\rangle - |-\alpha\rangle) ] \quad (68)$$

where  $|\pm\alpha\rangle = e^{\pm\frac{\eta\omega_0}{2}(b_0-b_0^\dagger)}|0\rangle$ . This corresponds to a maximally entangled state for which measurements of  $\sigma_x$  yield orthogonal Schrödinger cat-states of the resonator.

#### 4. Conclusions and outlook

In conclusion, we set forth a scheme for inducing strong optomechanical effects in suspended CNTs via the deformation potential exciton-phonon coupling. This provides an alternative to radiation-pressure based schemes [4, 5, 6] for an ultra-low mass and high frequency nanoscale resonator leading to large backaction-cooling factors and opening a direct route to the quantum behaviour of a “macroscopic” mechanical degree of freedom as it affords a mechanical analogue of cavity-QED [1, 2]. Most importantly, these breakthroughs rely on a lifetime-limited zero phonon line much narrower than the smallest CNT linewidths reported so far [23]. Indeed, the envisaged NTQDs will allow us to suppress the two most likely linewidth-broadening mechanisms, namely: inhomogeneous broadening and phonon-induced dephasing [70], by providing a controlled electrostatic environment and strong confinement of low-frequency phonons. Beyond nanomechanical applications, a doped version of these NTQDs will enable a tunable spin-photon interface [71]. Our technique could also apply to other high quality one-dimensional semiconductors such as prismatic nanowires [72]. Lastly, the simple approximation [Eq. (36)] we have derived for the deformation potential of a confined  $E_{11}$  direct exciton subjected to a transverse electric field will further the understanding of electron-phonon interactions in these CNT systems.

IWR acknowledges helpful discussions with Naser Qureshi, Adrian Bachtold and Peter Rabl, and financial support from Nanosystems Initiative Munich and DFG grant WI-3859/1-1.

#### References

- [1] Armour A D, Blencowe M P and Schwab K C 2002 *Phys. Rev. Lett.* **88** 148301
- [2] Blencowe M 2004 *Phys. Rep.* **395**(3) 159
- [3] Schwab K C and Roukes M L 2005 *Physics Today* **58** 36
- [4] Kippenberg T J and Vahala K J 2008 *Science* **321** 1172
- [5] Marquardt F and Girvin S M 2009 *Physics* **2** 40
- [6] Favero I and Karrai K 2009 *Nature Photon.* **3**(4) 201
- [7] Aspelmeyer M, Meystre P and Schwab K 2012 *Physics Today* **65** 29–35
- [8] O’Connell A D, Hofheinz M, Ansmann M, Bialczak R C, Lenander M, Lucero E, Neeley M, Sank D, Wang H, Weides M, Wenner J, Martinis J M and Cleland A N 2010 *Nature* **464** 697–703
- [9] Rocheleau T, Ndukum T, Macklin C, Hertzberg J B, Clerk A A and Schwab K C 2010 *Nature* **463** 72–75
- [10] Teufel J D, Donner T, Li D, Harlow J W, Allman M S, Cicak K, Sirois A J, Whittaker J D, Lehnert K W and Simmonds R W 2011 *Nature* **475** 359–363

- [11] Chan J, Alegre T P M, Safavi-Naeini A H, Hill J T, Krause A, Groblacher S, Aspelmeyer M and Painter O 2011 *Nature* **478** 89–92
- [12] Verhagen E, Deleglise S, Weis S, Schliesser A and Kippenberg T J 2012 *Nature* **482** 63–67
- [13] Sazonova V, Yaish Y, Üstünel H, Roundy D, Arias T A and McEuen P L 2004 *Nature* **431** 284
- [14] Tian L and Zoller P 2004 *Phys. Rev. Lett.* **93** 266403
- [15] Zippilli S, Morigi G and Bachtold A 2009 *Phys. Rev. Lett.* **102** 096804
- [16] Leturcq R, Stampfer C, Inderbitzin K, Durrer L, Hierold C, Mariani E, Schultz M G, von Oppen F and Ensslin K 2009 *Nat. Phys.* **5**(5) 327
- [17] Steele G A, Huttel A K, Witkamp B, Poot M, Meerwaldt H B, Kouwenhoven L P and van der Zant H S J 2009 *Science* **325** 1103
- [18] Lassagne B, Tarakanov Y, Kinaret J, Garcia-Sanchez D and Bachtold A 2009 *Science* **325** 1107
- [19] Huttel A K, Steele G A, Witkamp B, Poot M, Kouwenhoven L P and van der Zant H S J 2009 *Nano Lett.* **9**(7) 2547
- [20] Favero I, Stapfner S, Hunger D, Paulitschke P, Reichel J, Lorenz H, Weig E M and Karrai K 2009 *Opt. Express* **17** 12813–12820
- [21] Anetsberger G, Arcizet O, Unterreithmeier Q P, Riviere R, Schliesser A, Weig E M, Kotthaus J P and Kippenberg T J 2009 *Nature Phys.* **5**(12) 909
- [22] Favero I and Karrai K 2008 *New J. Phys.* **10** 095006
- [23] Htoon H, O’Connell M J, Cox P J, Doorn S K and Klimov V I 2004 *Phys. Rev. Lett.* **93** 027401
- [24] Högele A, Galland C, Winger M and Imamoglu A 2008 *Phys. Rev. Lett.* **100** 217401
- [25] Torrens O N, Zheng M and Kikkawa J M 2008 *Phys. Rev. Lett.* **101** 157401
- [26] Srivastava A, Htoon H, Klimov V I and Kono J 2008 *Phys. Rev. Lett.* **101** 087402
- [27] Suzuura H and Ando T 2002 *Phys. Rev. B* **65** 235412
- [28] Mariani E and von Oppen F 2009 *Phys. Rev. B* **80**(15) 155411
- [29] Högele A, Seidl S, Kroner M, Karrai K, Warburton R J, Gerardot B D and Petroff P M 2004 *Phys. Rev. Lett.* **93** 217401
- [30] Gerritsma R, Kirchmair G, Zahringer F, Solano E, Blatt R and Roos C F 2010 *Nature* **463** 68–71
- [31] Clerk A A, Devoret M H, Girvin S M, Marquardt F and Schoelkopf R J 2010 *Rev. Mod. Phys.* **82** 1155–1208
- [32] Wilson-Rae I, Zoller P and Imamoglu A 2004 *Phys. Rev. Lett.* **92** 075507
- [33] Thompson R J, Rempe G and Kimble H J 1992 *Phys. Rev. Lett.* **68** 1132–1135
- [34] Gleyzes S, Kuhr S, Guerlin C, Bernu J, Deleglise S, Busk Hoff U, Brune M, Raimond J M and Haroche S 2007 *Nature* **446**(7133) 297
- [35] Courty J M, Heidmann A and Pinard M 2001 *Eur. Phys. J. D* **17** 399
- [36] Vitali D, Mancini S, Ribichini L and Tombesi P 2002 *Phys. Rev. A* **65** 063803
- [37] Petroff P M, Lorke A and Imamoglu A 2001 *Phys. Today* **54** 46
- [38] Ohlsson N, Nilsson M and Kröll S 2003 *Phys. Rev. A* **68** 063812
- [39] de Riedmatten H, Afzelius M, Staudt M U, Simon C and Gisin N 2008 *Nature* **456** 773
- [40] Jelezko F, Volkmer A, Popa I, Rebane K K and Wrachtrup J 2003 *Phys. Rev. A* **67** 041802
- [41] Gaebel T, Domhan M, Popa I, Wittmann C, Neumann P, Jelezko F, Rabeau J R, Stavrias N, Greentree A D, Prawer S, Meijer J, Twamley J, Hemmer P R and Wrachtrup J 2006 *Nature Phys.* **2** 408
- [42] DiVincenzo D P and Mele E J 1984 *Phys. Rev. B* **29** 1685
- [43] Ando T 2006 *J. Phys. Soc. Jpn.* **75** 024707
- [44] Jorio A, Fantini C, Pimenta M A, Capaz R B, Samsonidze G G, Dresselhaus G, Dresselhaus M S, Jiang J, Kobayashi N, Grüneis A and Saito R 2005 *Phys. Rev. B* **71** 075401
- [45] Chang E, Bussi G, Ruini A and Molinari E 2004 *Phys. Rev. Lett.* **92** 196401
- [46] Uryu S and Ando T 2006 *Phys. Rev. B* **74** 155411
- [47] Ando T 2004 *J. Phys. Soc. Jpn.* **73** 3351
- [48] Capaz R B, Spataru C D, Ismail-Beigi S and Louie S G 2006 *Phys. Rev. B* **74** 121401
- [49] Fagan J A, Simpson J R, Landi B J, Richter L J, Mandelbaum I, Bajpai V, Ho D L, Raffaele R,

- Walker A R H, Bauer B J and Hobbie E K 2007 *Phys. Rev. Lett.* **98** 147402
- [50] Barros E B, Jorio A, Samsonidze G G, Capaz R B, Souza Filho A G, Mendes Filho J, Dresselhaus G and Dresselhaus M S 2006 *Phys. Rep.* **431** 261
- [51] Araujo P T, Doorn S K, Kilina S, Tretiak S, Einarsson E, Maruyama S, Chacham H, Pimenta M A and Jorio A 2007 *Phys. Rev. Lett.* **98** 067401
- [52] Yakobson B I, Brabec C J and Bernholc J 1996 *Phys. Rev. Lett.* **76** 2511
- [53] Wilson-Rae I 2008 *Phys. Rev. B* **77** 245418
- [54] Lee C, Wei X, Kysar J W and Hone J 2008 *Science* **321** 385–388
- [55] Wilson-Rae I 2003 *Quantum dot-phonon interactions in semiconductor quantum optics* Ph.D. thesis University of California, Santa Barbara
- [56] Leggett A J, Chakravarty S, Dorsey A T, Fisher M P A, Garg A and Zwerger W 1987 *Rev. Mod. Phys.* **59** 1
- [57] Wilson-Rae I, Nooshi N, Dobrindt J, Kippenberg T and Zwerger W 2008 *New Journal of Physics* **10** 095007
- [58] Wilson-Rae I, Nooshi N, Zwerger W and Kippenberg T J 2007 *Phys. Rev. Lett.* **99** 093901
- [59] Marquardt F, Chen J P, Clerk A A and Girvin S M 2007 *Phys. Rev. Lett.* **99** 093902
- [60] Jaehne K, Hammerer K and Wallquist M 2008 *New J. Phys.* **10** 095019
- [61] Kilina S, Tretiak S, Doorn S K, Luo Z, Papadimitrakopoulos F, Piryatinski A, Saxena A and Bishop A R 2008 *Proc. Natl. Acad. Sci.* **105** 6797
- [62] Rabl P 2010 *Phys. Rev. B* **82**(16) 165320
- [63] Unterreithmeier Q P, Weig E M and Kotthaus J P 2009 *Nature* **458**(7241) 1001
- [64] Benedict L X, Louie S G and Cohen M L 1995 *Phys. Rev. B* **52** 8541
- [65] Fagan J A, Bajpai V, Bauer B J and Hobbie E K 2007 *App. Phys. Lett.* **91** 213105
- [66] Rips S, Kiffner M, Wilson-Rae I and Hartmann M J 2012 *New J. Phys.* **14** 023042
- [67] Braak D 2011 *Phys. Rev. Lett.* **107**(10) 100401
- [68] Dobrindt J M, Wilson-Rae I and Kippenberg T J 2008 *Phys. Rev. Lett.* **101** 263602
- [69] Emary C and Brandes T 2003 *Phys. Rev. E* **67**(6) 066203
- [70] Galland C, Högele A, Türeci H E and Imamoglu A 2008 *Phys. Rev. Lett.* **101** 067402
- [71] Galland C and Imamoglu A 2008 *Phys. Rev. Lett.* **101** 157404
- [72] Fontcuberta i Morral A, Spirkoska D, Arbiol J, Heigoldt M, Morante J R and Abstreiter G 2008 *Small* **4** 899